NORMAL BUTANE OXIDATION: MEASUREMENTS OF AUTOXIDATION PRODUCTS IN A JET-STIRRED REACTOR

Z Dbouk, N Belhadj, M Lailliau, R Benoit, G Dayma, P Dagaut

NORMAL BUTANE OXIDATION: MEASUREMENTS OF AUTOXIDATION PRODUCTS IN A JET-STIRRED REACTOR

Z. Dbouk[*,], N. Belhadj[*,**], M. Lailliau[*,**], R. Benoit[*], G. Dayma[*,**], P. Dagaut[*]**
philippe.dagaut@cnrs-orleans.fr
*CNRS-INSIS, ICARE, 1C avenue de la recherche scientifique, 45071 Orleans, France
**Université d'Orléans, Château de la Source, avenue du Parc Floral, 45067 Orléans, France

Abstract
The autoxidation of n-butane was studied experimentally in a jet-stirred reactor at 1 atm (560-720 K) and 10 atm (530-1030 K) for equivalence ratios in the range 0.25 to 1.5. Samples of reacting mixtures were analysed in the gas phase by gas chromatography using several detectors (Flame ionization detector, thermal conductivity detector, quadrupole mass spectrometer), hydrogen peroxide analyser, and Fourier transform infrared spectroscopy. In addition to the fuel and oxygen, 38 products were quantified. Liquid phase samples were obtained by trapping the reacting mixtures in cooled acetonitrile (273 K). The liquid samples were analysed by high resolution mass spectrometry (HRMS Orbitrap Q-Exactive), either after flow injection or separation by high pressure liquid chromatography (HPLC). Besides stable species, several other low-temperature oxidation products such as hydroperoxides and ketohydroperoxides, were detected. Products of third O_2 addition on fuel's radicals were also detected by high resolution mass spectrometry. A total of 9 chemical formulae representing several intermediates was detected. To assess the presence of hydroxyl or hydroperoxyl groups in the products of oxidation we performed H/D exchange with D_2O. Qualitative and quantitative results showed the same trends in terms of variation of mole fractions and signal intensities versus reacting temperature. Kinetic modelling was performed using a literature detailed kinetic reaction mechanism already used to simulate previous *n*-butane oxidation experiments in the cool-flame regime, showing that improvements are needed to better describe the oxidation of *n*-butane under the present conditions.

1. Introduction

n-Butane which has a research octane number of ~ 95 [1] is a minor component of natural gas; it is also present in liquefied gas from petroleum and gasoline [2]. The autoxidation of *n*-butane has already been the topic of many studies in the recent years [3-8]. However, few were devoted to the measurement or detection of elusive intermediate products of cool flames. *n*-Butane autoxidation has been studied in a jet-stirred reactor (JSR) at atmospheric pressure with molecular beam mass spectrometry and synchrotron vacuum UV photoionization [9]. The authors reported the variation of the formation of C_4-ketohydroperoxides (KHP), C_1-, C_2-, and C_4-hydroperoxides. Barhini et al. [5, 6] measured concentration profiles of hydrogen peroxide by cavity ring down spectroscopy (CRDS) in a JSR at atmospheric pressure. Blocquet et al. [8] measured the mole fractions of the hydroperoxyl radical in a JSR at atmospheric pressure using the indirect fluorescence assay by gas expansion technique. Djehiche et al. [4] measured directly the mole fractions of hydrogen peroxide and hydroperoxyl radicals in a JSR at atmospheric pressure. The experiments of Barhini et al. [5] were simulated by Ranzi et al. [10] who considered the Korcek mechanism which transforms γ-ketohydroperoxides into acids and carbonyl products through isomerization and decomposition [11-15]. In the case of *n*-butane, formic acid + acetone and acetic acid + acetaldehyde are expected products. However, none of these previous experimental works investigated the formation of products from a third O_2 addition on fuel's radicals, which has been demonstrated to occur several times in the recent

literature for a range of fuels including alkanes, aldehydes, esters, and ethers [16-27], and no isomer-resolved data have been reported so far for C_4-KHPs.

In the present work, we performed a series of *n*-butane oxidation experiments in a JSR at atmospheric pressure to complement those published earlier by Djehiche et al. [4]. We studied the formation of cool flame products, including products of third oxygen addition on fuel's radicals over a range of temperatures under these conditions. Quantification of chemical products was performed by gas chromatography and Fourier transform infrared spectroscopy. Experiments were also performed at 10 atm in a JSR where hydrogen peroxide and a large set of cool flame products were quantified using a range of analytical techniques. These experiments served to verify the quality of simulated results obtained using a reaction mechanism taken from the literature.

2. Experimental

The experiments were performed using a set-up allowing to study the oxidation of *n*-butane from 1 to 10 atm. A fused silica spherical JSR with a volume of 37 cm^3 was used. There, the stirring is achieved by 4 jets exiting 0.5 mm i.d. injectors nozzles. Details can be found in previous publications [28-30]. The mean residence time inside the reactor was 1.4 s at 10 atm and 6 s at 1 atm. These conditions were chosen in order to get enough fuel-conversion and be able to observe specific cool flame products. The temperature along the main axis of the reactor was measured by a movable Pt/Pt-Rh 10% thermocouple (0.1 mm in diameter) located inside a thin-wall fused silica housing. Temperature gradient was measured to be ~ 2 K cm^{-1}.

High-purity reactants from Air Liquide were oxygen (99.995% pure) and *n*-butane (>99.5% pure). They were diluted with nitrogen from Air Liquide (<5 ppm H_2, <50 ppm O_2, <100 ppm H_2O, <1000 ppm Ar) and mixed just before entering the injectors. For the 10 atm experiments, a cylinder containing 1% of *n*-butane in N_2 (Air Liquide) was used. The *n*-butane/nitrogen mixture was injected through a capillary and the O_2/N_2 mixture flowed in the reactor extension tube [30]. Mass flow controllers (Brooks 5850TR) were used for gas delivery. The gases were preheated before injection in the reactor to minimize temperature gradients inside the JSR. The experimental conditions are summarized in Table 1.

Table 1. Experimental conditions.

Parameters	1 atm experiments	10 atm experiments
Temperature range (K)	560-720	530-1030
Mean residence time (s)	6	1.4
Equivalence ratio	1	0.25, 1, 1.5
Initial mole fraction of *n*-butane	0.023	0.004
Initial mole fraction of O_2	0.1495	0.104, 0.026, 0.0173

Mole fractions of reactants and stable species formed during the autoxidation of *n*-butane at 1 and 10 atm were obtained using several instruments (gas chromatography with flame ionization detection–FID, thermal conductivity detection–TCD, and benchtop mass spectrometry–MS, online Fourier transform infrared spectroscopy–FTIR, online ATI hydrogen peroxide dual-channel monitor at 10 atm). The gas samples taken with a sonic probe were analysed online by FTIR and stored at 50 mbar in 1 L Pyrex bulbs for off-line gas chromatography analyses.

In addition, for the autoxidation experiments at 1 atm, samples were taken by bubbling oxidation samples in 20 mL of cool acetonitrile (0°C) for 75min. The solution obtained was analysed by flow injection (FIA) - Orbitrap Q-Exactive and liquid chromatography - Orbitrap

Q-Exactive. Two ionisation sources were used in positive and negative modes, i.e., atmospheric pressure chemical ionisation (APCI) and heated electrospray ionisation (HESI). A HPLC column (Acentis silica column from Supelco, 5µm, 100 Å, 250x2.1 mm) was used with an acetonitrile-water solvent (82.5% acetonitrile and 17.5% water). This procedure providing qualitative data is described at length in previous publications [17-19, 22, 24-26]. Because Orbitrap Q-Exactive cannot detect ions at m/z <50, M-$HCOO^-$ adduct ions were recorded. That way, H_2O_2 and C_1-C_3 products (CH_2O, CH_2O_2, C_2H_4O) were analysed. Ketohydroperoxides, butyl hydroperoxides or diols and diketones were analysed as a function of temperature, and products of third O_2 addition on fuel's radicals were detected. To assess the presence of OOH and/or OH functional groups in the products of oxidation, we performed OH/OD exchange. Here, 300 µL of D_2O (99.98% from Sigma-Aldrich) were introduced into 1 mL of liquid samples. We let H/D exchange to proceed for 20 min before analyses.

3. Kinetic modelling

Kinetic modelling was performed using the Chemkin II library [31]. We used the semi-detailed chemical kinetic reaction mechanism from Ranzi et al. [10] which takes into account the Korcek mechanism converting γ-ketohydroperoxides into acids and carbonyls. In that mechanism, butyl hydroperoxides, butyl ketohydroperoxides and cyclic ethers are represented by a single specie (C4H9OOH, NC4-OQOOH, C4H8O, respectively). The measured temperatures in JSR experiments were used as input in the PSR [32] computations.

4. Results and discussion

4.1 Oxidation at 10 atm

The results obtained under high pressure conditions (Table 1) consisted of mole fractions of the reactants (*n*-butane and oxygen), a large set of stable intermediates, and final products (carbon dioxide and water). Most of the chemical products were measured by FID after capillary column separation (50 m alumina column, 30 m and 3µm DB1 – 25 m and 1.2 µm CP-Sil 5CB, and 60 m DB624 capillary columns). A TCD was used to measure oxygen and hydrogen after separation on a 25 m Carboplot P7 column. FTIR was used to measure CO, CO_2, acids, and CH_2O (temperature-controlled gas cell: 140°C, 10 m pathlength, resolution of 0.5 cm^{-1}, 200 mbar of pressure). Calibrations were made by analysing standards. When standards could not be used in FID analyses, carbon-equivalent rules were applied [33]. Gas chromatography-mass spectrometry (GC-MS) was used for products identification (electron impact ionization at 70 eV). The quantified chemical species, besides the reactants, were final products and stables intermediates: H_2, H_2O, H_2O_2, CO_2, CO, CH_2O, CH_4, C_2H_2, C_2H_4, C_2H_6, oxirane, C_3H_6, trans 2-C_4H_8, cis 2-C_4H_8, 1-C_4H_8, 1,3-C_4H_6, CH_3CHO, methyl oxirane, 2-propenal, propanal, acetone, 2,3-dimethyl oxirane (cis and trans), ethyl oxirane, 2-methyl oxetane, furan, 2,3- and 2,5-dihydrofuran, methacrolein, butanal, 2,3-butanedione, 2-butanone, 3-buten-2-ol, methyl vinyl ketone, tetrahydrofuran (THF), formic acid, acetic acid. Figures 1a to 1f illustrate the results and presents a comparison of experimental and simulated mole fraction profiles under stoichiometric conditions.

Figure 1a shows that the model [10] overestimates the oxidation rate of the fuel in the negative temperature coefficient regime (NTC). The formation of water is too important in the cool flame, due to overproduction of hydroxyl radicals in relation to the overprediction of hydrogen peroxide by a factor of ca. 5 (Fig. 1b). Above ca. 750 K, the predicted formation of carbon dioxide and water is too important. Figure 1b shows that the model also tends to strongly overestimate the rate of oxidation of important intermediates such as ethylene, methane and propene. Acetaldehyde consumption rate above ca. 750 K is also overpredicted. Concerning carbonyl compounds (Fig. 1c), the model overestimates the production of acetone, butanal, and

2-butanone. The formation of 2,3-butanedione is relatively well predicted in the cool flame, but above 750 K, it is strongly underestimated. Acetic acid is well predicted in the cool flame (Fig. 1d), but not above ca. 800 K, whereas formic acid formation in the cool flame is overpredicted by a factor of ca. 2.5. Several C4-cyclic ethers were measured here (Fig. 1e). In the model, they are represented by a single product, C4H8O. One can see from Figure 1e that 2,3-dimethyl oxirane is the most important ether formed here. The observed order of importance is: 2,3-dimethyl oxirane (A) >> tetrahydrofuran (B) ≥ 2-methyloxetane (C) ≈ ethyloxirane (D).

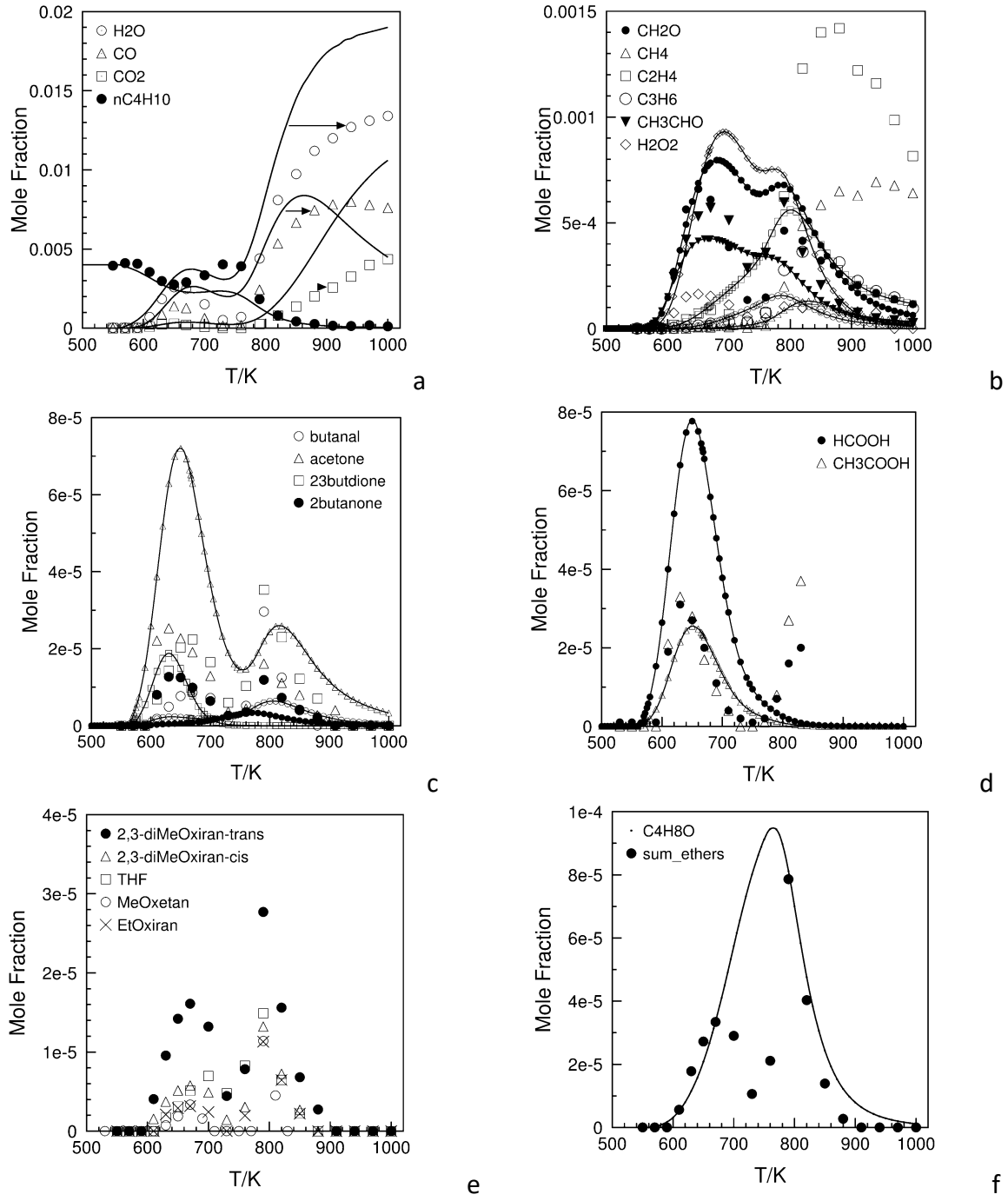

Figure 1 Comparison of experimental (symbols) and simulated (lines and small symbols) mole fractions of selected species measured during the oxidation of *n*-butane in a JSR under stoichiometric conditions at 10 atm (see Table 1).

The oxidation of 2-butyl can lead to the formation of all these isomers, except THF, whereas the oxidation of 1-butyl leads to the formation of tetrahydrofuran, 2-methyloxetane, and ethyloxirane:

1-butyl + O_2 → $^{\bullet}OOCH_2CH_2CH_2CH_3$ → $HOOCH_2CH_2CH_2^{\bullet}CH_2$ → B
→ $HOOCH_2CH_2^{\bullet}CHCH_3$ → C
→ $HOOCH_2^{\bullet}CHCH_2CH_3$ → D

2-butyl + O_2 → $CH_3CH_2CH(OO^{\bullet})CH_3$ → $CH_3^{\bullet}CHCH(OOH)CH_3$ → A
→ $^{\bullet}CH_2CHCH(OOH)CH_3$ → C
→ $CH_3CH_2CH(OOH)^{\bullet}CH_2$ → D

The sum of the mole fractions of these ethers was compared to the computed C4H8O mole fractions (Fig. 1f). Because the model does not predict a NTC as strong as in the experiments, it could represent only a fraction of the data (550-670 K and 800-900 K). Whereas pathways other than the Korcek mechanism could yield acetone, formic acid, acetaldehyde and acetic acid, as noticed at 10 atm in the cool flame, the two acids are produced in nearly equal quantities similar to acetone. Acetaldehyde maximum mole fraction is nearly 18 times higher. Reaction pathway analysis was performed at 640 K, showing that formic acid is produced via nC_4-OQOOH → HCOOH + CH_3COCH_3, acetaldehyde comes mainly from nC_4-OQOOH → CH_3CHO + 0.3 CH_3CO + 0.7 CH_2CHO + OH and OH + nC_4-OQOOH → H_2O + CH_2CO + CH_3CHO + OH (half importance), acetic acid is formed via nC_4-OQOOH → CH_3CHO + CH_3COOH, and acetone's overproduction is due to nC_4-OQOOH → HCOOH + CH_3COCH_3.

In summary, the model proposed by Ranzi et al.[10] describes only a fraction of the present data whereas it was previously shown to represent data obtained at atmospheric pressure. Nevertheless, we further used that mechanism for simulating experiments performed at 1 atm (Section 4.2).

4.2 Oxidation at 1 atm

In addition to chromatographic and FTIR analyses (see Section 3.1 for details), qualitative measurements were made by Orbitrap. They consisted of ions signal profiles obtained for samples taken as a function of JSR temperature and constant residence time. FIA and HPLC were used. M-$HCOO^-$ adduct ions were recorded (APCI in negative ionisation mode) for low-mass products: H_2O_2, CH_2O, C_2H_4O. Ketohydroperoxides (KHP, $C_4H_8O_3$), butylhydroperoxides ($C_4H_{10}O_2$) and butanediones ($C_4H_6O_2$) resulting from ketohydroperoxides decomposition were measured, as well as $C_4H_8O_5$, produced via third O_2 addition on fuel's radicals. That last product was too low in concentration to present data as a function of JSR temperature. The formation of ketohydroperoxides occurs via the addition of two molecules of oxygen on the fuel's radicals: $C_4H_9^{\bullet}$ + O_2 → $C_4H_9OO^{\bullet}$ followed by H-atom transfer yielding $^{\bullet}C_4H_8OOH$ which reacts with oxygen and, after H-atom transfer, decomposes to form a KHP, i.e., $^{\bullet}C_4H_8OOH$ + O_2 → $^{\bullet}OOC_4H_8OOH$ → $^{\bullet}C_4H_7(OOH)_2$ → $C_4H_8O_3$ + $^{\bullet}OH$. Six different KHPs can be produced during the oxidation of *n*-butane. Our HPLC-Orbitrap APCI (–) analyses demonstrated the presence of a major chromatographic peak and of four other lower intensity peaks (Fig. 2). Coelution of the main chromatographic peak could not be avoided. It could be due to KHPs arising from the peroxidation of 1-butyl and 2-butyl radicals, i.e., $CH_3(C{=}O)CH_2CH_2OOH$ and $CH_3CH(OOH)CH_2CH(=O)$, respectively. The isomers could not be identified due to the formation of too similar fragments (fragmentation energy of 10 eV).

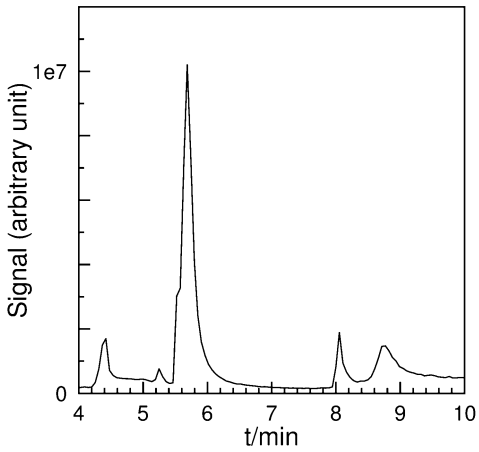

Figure 2. Separation of ketohydroperoxides by liquid chromatography and detection by Orbitrap. Sample taken at 1 atm, 600 K. APCI(–) was used; ionic signal at m/z 103.03880. is plotted.

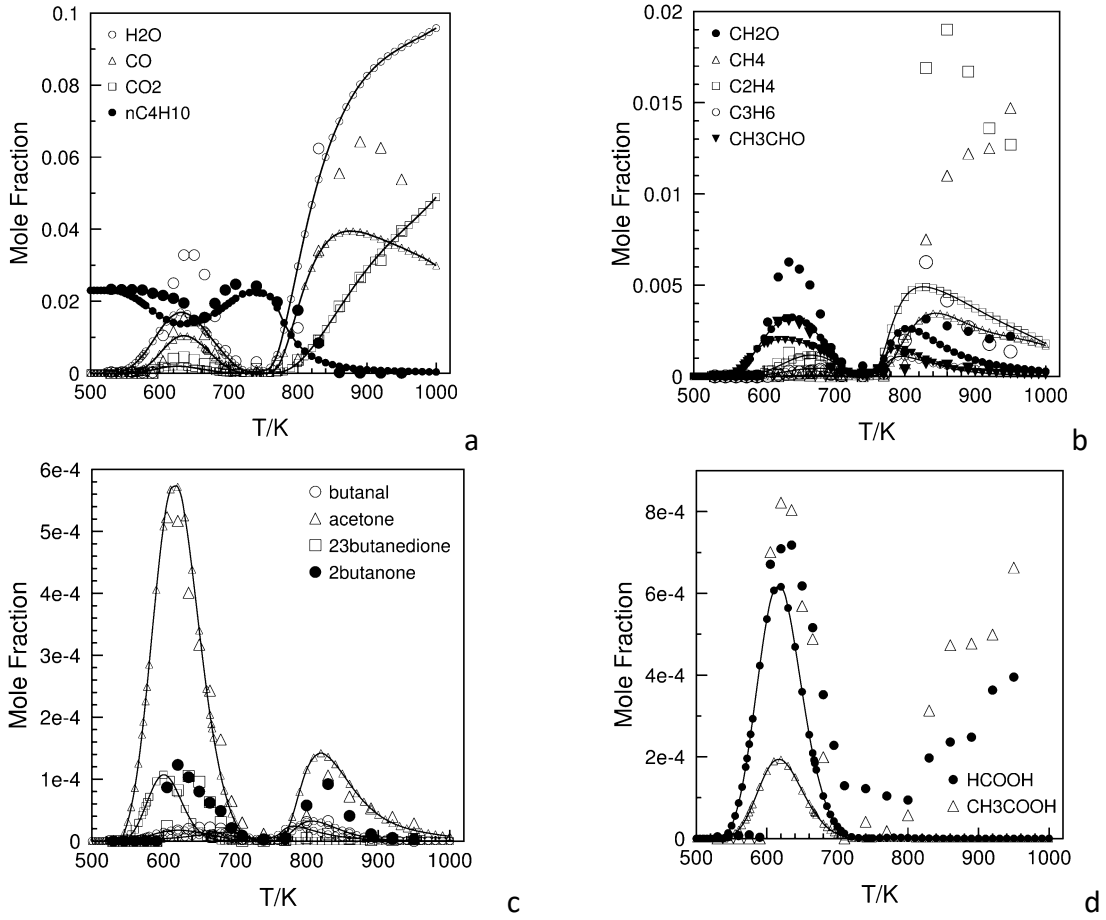

Figure 3 Comparison of experimental (symbols) and simulated (lines and small symbols) mole fractions of selected species measured during the oxidation of *n*-butane in a JSR under stoichiometric conditions at 1 atm (see Table 1).

Figures 3 to 4 present the experimental results obtained here. When possible, the present data are compared to (i) our previous data obtained by CRDS and (ii) modelling results. Figure 3a shows that the model overestimates the fuel oxidation rate below 700 K although the formation of water is underestimated in the cool flame. The production of CO and CO_2 is also underestimated by the model in the cool flame. Above 800 K, the model better represents the

data. Figure 3b shows that formation of formaldehyde and that of acetaldehyde are underestimated by the model in the cool flame.

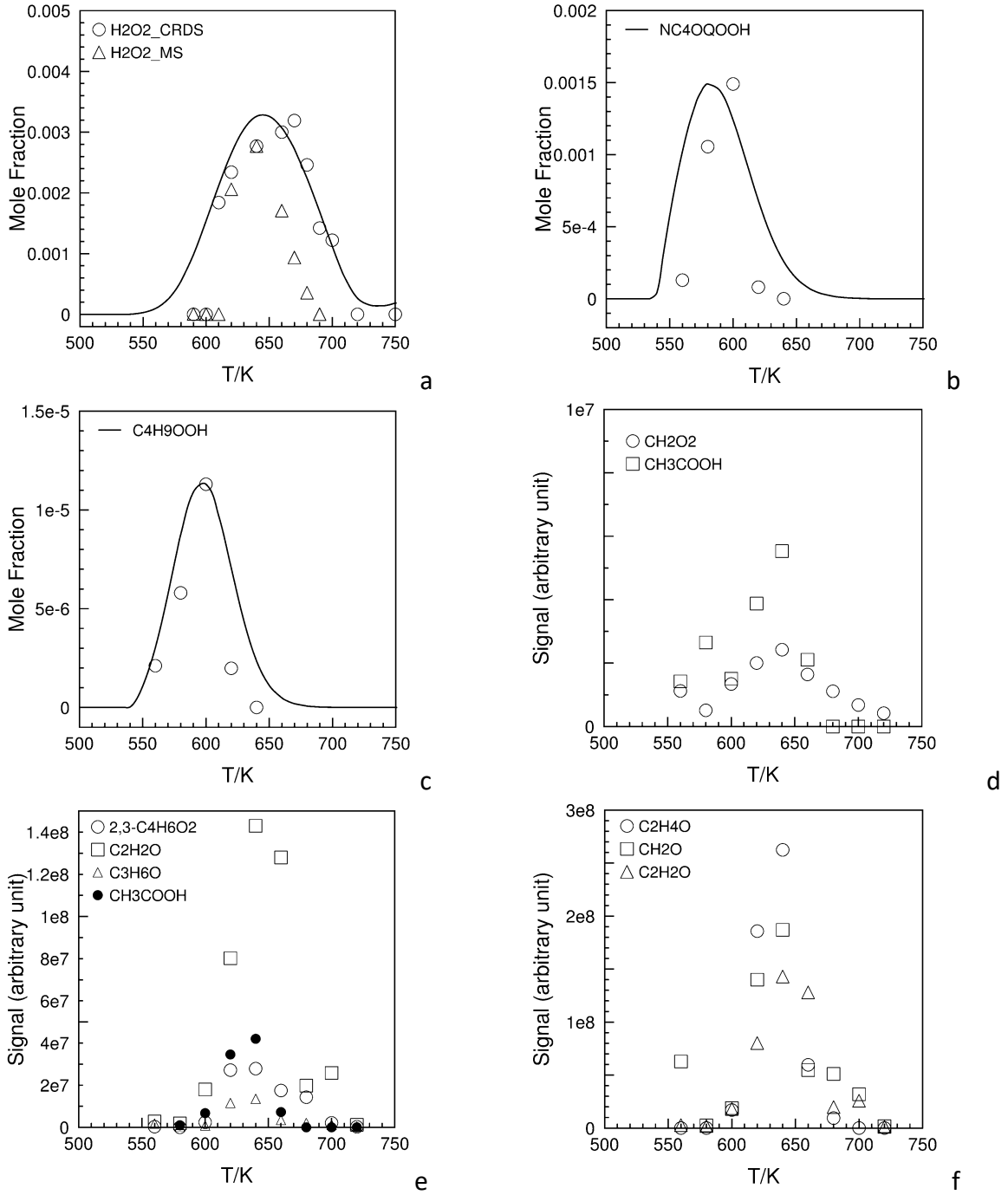

Figure 4 Comparison of experimental (symbols) and simulated (lines) mole fractions of selected species measured during the oxidation of *n*-butane in a JSR under stoichiometric conditions at 1 atm (see Table 1).

Above 800 K, discrepancies between data and simulated mole fraction are observed for all the intermediate products. Figure 3c presents the results obtained for acetone and C_4-carbonyls. One can see that acetone formation is well predicted over the entire temperature range of this study. The production of 2,3-butanedione and that of butanal are predicted well, but the model fails to predict the formation of 2-butanone (17.5 ppm predicted at 620 K vs.123 ppm measured at 620 K). On Figure 3d, products of the Korcek mechanism are plotted. Whereas

other routes than the Korcek mechanism can yield acetone, formic acid, acetaldehyde and acetic acid, it is interesting to note that in the cool flame, the two acids are produced in nearly equal quantities, also very close to that of acetone. Acetaldehyde maximum mole fraction is c.a. 4 times higher. In the cool flame, the formation of formic acid is well predicted whereas that of acetic acid is underestimated by a factor of ca. 4. At 600 K, a rate of production analysis was performed. It indicated that formic acid comes from the decomposition of C_4 KHPs: nC_4-OQOOH → HCOOH + CH_3COCH_3 (Korcek mechanism). In the model, acetaldehyde is mainly formed by two reactions of equal importance: nC_4-OQOOH → CH_3CHO + 0.3 CH_3CO +0.7 CH_2CHO + OH and nC_4-OQOOH → H_2O + CH_2CO + CH_3CHO + OH. In the computations, acetic acid is formed through the decomposition of C_4-KHPs: nC_4-OQOOH → CH_3CHO + CH_3COOH (Korcek mechanism). In the simulations, acetone is essentially formed through the decomposition of C_4-KHPs: nC_4-OQOOH → HCOOH + CH_3COCH_3 (Korcek mechanism).

Figure 4 presents the HRMS data compared to simulations for selected products. In Fig. 4a, HRMS data were scaled to CRDS data at 640 K; analyses were performed using HPLC-HRMS APCI (–); the signal corresponds to m/z 79.0022 for H_2O_2 with $HCOO^-$ adduct. In Fig. 4b, HRMS data were scaled to simulated maximum mole fraction. Analyses were carried out by FIA- APCI (+); the signal at m/z 105.05484 is plotted. In Fig. 4c, HRMS data were scaled to simulations. Analyses were performed by FIA-APCI (+); the signal at m/z 91.07576 is plotted. In Fig. 4d to 4f, raw ionic signals are presented. In Fig. 4d, CH_2O_2 is detected with a $HCOO^-$ adducts. Analyses of CH_2O_2 were performed using HPLC-HRMS APCI (–); the signal at m/z 91.0021 is plotted. For CH_3COOH analysis, we used HESI (–) HPLC-HRMS; the signal at m/z 59.0124 is presented. In Fig. 4e C_2H_2O and CH_3COOH are detected with $HCOO^-$ adducts. The analyses of C_2H_2O were carried out using APCI (–) HPLC-HRMS (signal at m/z 87.0072). The analyses of $C_4H_6O_2$ and C_3H_6O were performed using APCI (+) HPLC-HRMS (signal at m/z 87.0447 and m/z 59.0500, respectively). The analysis of CH_3COOH was performed by HESI (–) HPLC-HRMS (signal at m/z 105.0176).

In Fig. 4f, C_2H_4O, CH_2O, and C_2H_2O were detected with $HCOO^-$ adducts using APCI (–) HPLC-HRMS (signal at m/z 89.0228, m/z 75.0072, and m/z 87.0072, respectively). Figure 4a shows a comparison of quantitative measurements of hydrogen peroxide by CRDS [4], qualitative HRMS measurement, and computed mole fractions using the model of Ranzi et al. The HRMS data were scaled to the CRDS data at 640 K. One can see good agreement between all the mole fraction profiles. Figure 4b shows the simulated KHP mole fractions compare to HRMS data scaled to the maximum computed mole fraction. From that figure, one can observe a good match between data and modelling. This is also the case for $C_4H_{10}O_2$ (butylhydroperoxides and diols) when HRMS data are scaled to the maximum computed mole C_4H_9OOH fraction. APCI and HESI were used to track a set of other species.

The present results are presented in Figures 4d, e, f. From these figures, one can see that all the products present a maximum signal intensity at 640 K, as observed in corresponding GC analyses of most of the intermediate cool flame products. Molecular formulae can correspond to several isomers, e.g., C_2H_4O. However, one can estimate that CH_2O_2 represents formic acid, CH_2O represents formaldehyde, C_2H_2O represents ketene, $C_2H_4O_2$ represents acetic acid, C_3H_6O represents mostly acetone, and C_2H_4O represents mainly acetaldehyde (~64% acetaldehyde and ~36% oxirane). The profile for 2,3-$C_4H_6O_2$ was obtained by HPLC-HRMS after identification using a 2,3-butanedione standard.

In order to further characterise the cool flame products, we performed H/D exchange with D_2O to assess the presence of hydroxyl or hydroperoxyl groups in the products (Table 2). Analyses were performed in FIA/APCI (+/–) modes. For KHPs, a strong H/D exchange was observed as shown in Table 2. $C_4H_6O_2$ corresponds to several isomers. Butanediones were identified by GC-MS. Because two H/D exchanges were observed here, unsaturated diols are likely present in the analysed sample. Many isomers can correspond to C_4H_8O. In this work,

cyclic ethers, ketones, aldehydes, and unsaturated alcohols have been identified by GC-MS. Among this species, only unsaturated alcohols could form deuterated products in presence of D_2O. Here, the observation of $C_4H_7D_1O$ indicates their likely presence in the oxidation products. C4H8O2 could represent butyric acid and unsaturated hydroperoxides. Because $C_4H_7D_1O_2$ was observed, the presence of unsaturated ROOH in the analysed sample is likely (butyric acid shows no H/D exchange in presence of D_2O [17]). $C_4H_{10}O_2$ can represent diols and ROOH. The strong signal observed for $C_4H_8D_2O_2^+$ indicates the likely presence of diols in the sample.

Table 2. H/D exchange results for products of *n*-butane oxidation in a JSR at 640K and 1 atm.

M (g/mol)	Species		APCI (+)		APCI (–)	
	Formula	Possible isomers	m/z $(M+H)^+$	Signal (a.u)	m/z $(M-H)^-$	Signal (a.u)
72	C_4H_8O	cyclic ether ketones aldehydes unsaturated alcohol	73.06538	1.02E8	71.04977	2.87E5
73	$C_4H_7D_1O$	unsaturated alcohol	74.07173	8.90E7	72.05535	4.11E4
86	$C_4H_6O_2$	dione or unsaturated diols	87.04385	2.93E8	85.02824	5.59E6
87	$C_4H_5D_1O_2$	unsaturated diols	88.05024	4.32E7	86.03459	5.18E6
88	$C_4H_4D_2O_2$	unsaturated diols	89.05715	1.80E7	87.04084	8.90E4
88	$C_4H_8O_2$	butyric acid or unsaturated ROOH	89.06010	2.38E7	87.04451	3.34E5
89	$C_4H_7D_1O_2$	idem	90.06646	2.30E7	88.05024	3.60E5
90	$C_4H_6D_2O_2$	idem	91.07281	2.46E6	89.05647	2.51E5
90	$C_4H_{10}O_2$	ROOH or diols	91.07575	9.45E6	89.05959	1.95E5
91	$C_4H_9D_1O_2$	idem	92.08211	1.06E7	-	-
92	$C_4H_8D_2O_2$	diols	93.08837	3.25E6	-	-
104	$C_4H_8O_3$	KHPs or keto-diols	105.05444	7.32E6	103.03880	7.67E7
105	$C_4H_7D_1O_3$	KHPs or keto-diols	106.06120	1.16E7	104.04517	7.77E7
106	$C_4H_6D_2O_3$	keto-diols	107.0674	7.14E6	105.05139	5.40E4
136	$C_4H_8O_5$	keto-dihydroperoxide	137.04578	1.54E4	135.02859	2.01E5
137	$C_4H_7D_1O_5$	idem	-	-	136.03522	9.41E5
138	$C_4H_6D_2O_5$	idem	-	-	137.04152	9.84E5

If the second H-atom transfer in a peroxy-alkylhydroperoxide radical does not occur on the C-atom bonded to the OOH group, a third O_2 addition can occur and yield a keto-alkyl-dihydroperoxide:

$$^{\bullet}OOC_4H_8OOH \rightarrow {}^{\bullet}C_4H_7(OOH)_2$$
$$^{\bullet}C_4H_7(OOH)_2 + O_2 \rightarrow {}^{\bullet}OOC_4H_7(OOH)_2 \rightarrow {}^{\bullet}OH + O{=}C_4H_6(OOH)_2.$$

Only a small signal of the corresponding ion $C_4H_9O_5^+$ was observed under the present conditions with positive APCI ionisation. We performed H/D exchange with D_2O to verify the presence of two hydroperoxyl groups in $C_4H_8O_5$. As can be seen from Table 2, $C_4H_5D_2O_5^-$ could be observed, confirming the formation of a keto-alkyl-dihydroperoxide.

5. Conclusion

New experimental results were obtained in a JSR at 1 and 10 atm, using a range of analytical techniques: gas chromatography with flame ionization detector, thermal conductivity detector, quadrupole mass spectrometry, hydrogen peroxide analyser, Fourier transform infrared spectrometry, liquid chromatography and high-resolution mass spectrometry (Orbitrap Q-Exactive). H/D exchange with D_2O was used to assess the presence of hydroxyl or hydroperoxyl groups in the products. The large set of qualitative and quantitative data obtained here was combined with published results obtained under the same experimental conditions at 1 atm, and simulated. A kinetic reaction mechanism which takes into account the Korcek mechanism was taken from the literature and used to simulate the present experiments. Reaction pathway analyses revealed that in the model the reactions of the Korcek mechanism are mostly contributing to the formation of formic acid, acetic acid, and acetone at 1 and 10 atm, but not acetaldehyde. This study showed that the selected kinetic model only partially represents the data and should be improved, both under cool flame and high temperature conditions.

Acknowledgements
Support from the CAPRYSSES project (ANR- 11-LABX-006–01) funded by ANR through the PIA (Programme d'Investissement d'Avenir) is gratefully acknowledged. Help from C. Togbé and F. Karsenty for the JSR experiments is gratefully acknowledged.

References

[1] Guibet, J.C., "Fuels and Engines. Technology - Energy - Environment". Editions Technip: Paris, 1999, p. 786.
[2] Speight, J., in: J. Speight (Ed.) Shale Oil and Gas Production Processes, Gulf Professional Publishing: 2020.
[3] Xu, Q., Liu, B.Z., Chen, W.Y., Yu, T.P., Zhang, Z.H., Zhang, C., Wei, L.X., Wang, Z.D., "Comprehensive study of the low-temperature oxidation chemistry by synchrotron photoionization mass spectrometry and gas chromatography", *Combust. Flame* 236: 11797-11797 (2022).
[4] Djehiche, M., Le Tan, N.L., Jain, C.D., Dayma, G., Dagaut, P., Chauveau, C., Pillier, L., Tomas, A., "Quantitative Measurements of HO2 and Other Products of n-Butane Oxidation (H2O2, H2O, CH2O, and C2H4) at Elevated Temperatures by Direct Coupling of a Jet-Stirred Reactor with Sampling Nozzle and Cavity Ring-Down Spectroscopy (cw-CRDS)", *J. Am. Chem. Soc.* 136: 16689-16694 (2014).
[5] Bahrini, C., Morajkar, P., Schoemaecker, C., Frottier, O., Herbinet, O., Glaude, P.-A., Battin-Leclerc, F., Fittschen, C., "Experimental and modeling study of the oxidation of n-butane in a jet stirred reactor using cw-CRDS measurements", *Phys. Chem. Chem. Phys.* 15: 19686-19698 (2013).
[6] Bahrini, C., Herbinet, O., Glaude, P.A., Schoemaecker, C., Fittschen, C., Battin-Leclerc, F., "Quantification of Hydrogen Peroxide during the Low-Temperature Oxidation of Alkanes", *J. Am. Chem. Soc.* 134: 11944-11947 (2012).
[7] Herbinet, O., Battin-Leclerc, F., Bax, S., Le Gall, H., Glaude, P.-A., Fournet, R., Zhou, Z., Deng, L., Guo, H., Xie, M., Qi, F., "Detailed product analysis during the low temperature oxidation of n-butane", *Phys. Chem. Chem. Phys.* 13: 296-308 (2011).
[8] Blocquet, M., Schoemaecker, C., Amedro, D., Herbinet, O., Battin-Leclerc, F., Fittschen, C., "Quantification of OH and HO2 radicals during the low-temperature oxidation of hydrocarbons by Fluorescence Assay by Gas Expansion technique", *Proc. Natl. Acad. Sci. U. S. A.* 110: 20014-20017 (2013).

[9] Battin-Leclerc, F., Herbinet, O., Glaude, P.-A., Fournet, R., Zhou, Z., Deng, L., Guo, H., Xie, M., Qi, F., "New experimental evidences about the formation and consumption of ketohydroperoxides", *Proc. Combust. Inst.* 33: 325-331 (2011).
[10] Ranzi, E., Cavallotti, C., Cuoci, A., Frassoldati, A., Pelucchi, M., Faravelli, T., "New reaction classes in the kinetic modeling of low temperature oxidation of n-alkanes", *Combust. Flame* 162: 1679-1691 (2015).
[11] Jalan, A., Alecu, I.M., Meana-Paneda, R., Aguilera-Iparraguirre, J., Yang, K.R., Merchant, S.S., Truhlar, D.G., Green, W.H., "New Pathways for Formation of Acids and Carbonyl Products in Low-Temperature Oxidation: The Korcek Decomposition of gamma-Ketohydroperoxides", *J. Am. Chem. Soc.* 135: 11100-11114 (2013).
[12] Zinbo, M., Jensen, R.K., Korcek, S., "Gas-liquid-chromatography of oxygenated compounds related to autoxidation of n-hexadecane", *Anal. Lett.* 10: 119-132 (1977).
[13] Jensen, R.K., Korcek, S., Mahoney, L.R., Zinbo, M., "Liquid-phase autoxidation of organic-compounds at elevated-temperatures .1. stirred flow reactor technique and analysis of primary products from normal-hexadecane autoxidation at 120-degrees-C 180-degrees-C", *J. Am. Chem. Soc.* 101: 7574-7584 (1979).
[14] Jensen, R.K., Korcek, S., Mahoney, L.R., Zinbo, M., "Liquid-phase autoxidation of organic-compounds at elevated-temperatures .2. Kinetics and mechanisms of the formation of cleavage products in normal-hexadecane autoxidation", *J. Am. Chem. Soc.* 103: 1742-1749 (1981).
[15] Jensen, R.K., Zinbo, M., Korcek, S., "HPLC determination of hydroperoxidic products formed in the autoxidation of normal-hexadecane at elevated-temperatures", *J. Chromatogr. Sci.* 21: 394-397 (1983).
[16] Wang, Z., Popolan-Vaida, D.M., Chen, B., Moshammer, K., Mohamed, S.Y., Wang, H., Sioud, S., Raji, M.A., Kohse-Höinghaus, K., Hansen, N., Dagaut, P., Leone, S.R., Sarathy, S.M., "Unraveling the structure and chemical mechanisms of highly oxygenated intermediates in oxidation of organic compounds", *Proceedings of the National Academy of Sciences* 114: 13102-13107 (2017).
[17] Belhadj, N., Benoit, R., Dagaut, P., Lailliau, M., Serinyel, Z., Dayma, G., Khaled, F., Moreau, B., Foucher, F., "Oxidation of di-n-butyl ether: Experimental characterization of low-temperature products in JSR and RCM", *Combust. Flame* 222: 133-144 (2020).
[18] Belhadj, N., Benoit, R., Dagaut, P., Lailliau, M., "Experimental characterization of n-heptane low-temperature oxidation products including keto-hydroperoxides and highly oxygenated organic molecules (HOMs)", *Combust. Flame* 224: 83-93 (2021).
[19] Belhadj, N., Benoit, R., Dagaut, P., Lailliau, M., "Experimental Characterization of Tetrahydrofuran Low-Temperature Oxidation Products Including Ketohydroperoxides and Highly Oxygenated Molecules", *Energy Fuels* 35: 7242–7252 (2021).
[20] Belhadj, N., Benoit, R., Dagaut, P., Lailliau, M., Moreau, B., Foucher, F., "Low-temperature oxidation of a gasoline surrogate: Experimental investigation in JSR and RCM using high-resolution mass spectrometry", *Combust. Flame* 228: 128-141 (2021).
[21] Belhadj, N., Benoit, R., Dagaut, P., Lailliau, M., Serinyel, Z., Dayma, G., "Oxidation of di-n-propyl ether: Characterization of low-temperature products", *Proc. Combust. Inst.* 38: 337-344 (2021).
[22] Belhadj, N., Benoit, R., Lailliau, M., Glasziou, V., Dagaut, P., "Oxidation of diethyl ether: Extensive characterization of products formed at low temperature using high resolution mass spectrometry", *Combust. Flame* 228: 340-350 (2021).
[23] Belhadj, N., Lailliau, M., Benoit, R., Dagaut, P., "Experimental and kinetic modeling study of n-hexane oxidation. Detection of complex low-temperature products using high-resolution mass spectrometry", *Combust. Flame* 233: 111581 (2021).

[24] Belhadj, N., Lailliau, M., Benoit, R., Dagaut, P., "Towards a Comprehensive Characterization of the Low-Temperature Autoxidation of Di-n-Butyl Ether", *Molecules* 26: 7174 (2021).
[25] Belhadj, N., Lailliau, M., Benoit, R., Dagaut, P., "Experimental and kinetic modeling study of n-pentane oxidation at 10 atm, Detection of complex low-temperature products by Q-Exactive Orbitrap", *Combust. Flame* 235: 11723-11723 (2022).
[26] Belhadj, N., Lailliau, M., Dbouk, Z., Benoit, R., Moreau, B., Foucher, F., Dagaut, P., "Gasoline Surrogate Oxidation in a Motored Engine, a JSR, and an RCM: Characterization of Cool-Flame Products by High-Resolution Mass Spectrometry", *Energy Fuels* 36: 3893-3908 (2022).
[27] Chen, W., Xu, Q., Lou, H., Di, Q., Xie, C., Liu, B., Yang, J., Gall, H.L., Tran, L.S., Wang, X., Xia, Z., Herbinet, O., Battin-Leclerc, F., Wang, Z., "Variable pressure JSR study of low temperature oxidation chemistry of n-heptane by synchrotron photoionization mass spectrometry", *Combust. Flame* 240: 111946 (2022).
[28] Dagaut, P., Cathonnet, M., Rouan, J.P., Foulatier, R., Quilgars, A., Boettner, J.C., Gaillard, F., James, H., "A jet-stirred reactor for kinetic studies of homogeneous gas-phase reactions at pressures up to ten atmospheres (≈1 MPa)", *Journal of Physics E: Scientific Instruments* 19: 207-209 (1986).
[29] Dagaut, P., Cathonnet, M., Boettner, J.C., Gaillard, F., "Kinetic modeling of ethylene oxidation", *Combust. Flame* 71: 295-312 (1988).
[30] Le Cong, T., Dagaut, P., Dayma, G., "Oxidation of Natural Gas, Natural Gas/Syngas Mixtures, and Effect of Burnt Gas Recirculation: Experimental and Detailed Kinetic Modeling", *Journal of Engineering for Gas Turbines and Power* 130: 041502-10 (2008).
[31] Kee, R.J., Rupley, F.M., Miller, J.A., "CHEMKIN-II: A Fortran Chemical Kinetics Package for the Analysis of Gas-Phase Chemical Kinetics.", Sandia National Laboratories, Livermore, CA, 1989.
[32] Glarborg, P., Kee, R.J., Grcar, J.F., Miller, J.A., "PSR: A FORTRAN program for modeling well-stirred reactors.", SAND86-8209, Sandia National Laboratories, Livermore, CA, 1986.
[33] Schofield, K., "The enigmatic mechanism of the flame ionization detector: Its overlooked implications for fossil fuel combustion modeling", *Prog. Energy Combust. Sci.* 34: 330-350 (2008).

Supplementary Material

Table S1. APCI settings for FIA and HPLC-MS analyses

	FIA	**HPLC**
Syringe or mobile phase flow rate (µl/min)	5-7	170
Sheath gas flow (a.u)	10	50
Auxiliary gas flow (a.u)	1	0
Sweep gas flow (a.u)	0	0
Capillary temperature (°C)	200	300
Vaporizer temperature (°C)	120	120
Corona discharge current (µA)	4 to 5.5	4 to 5
Spray voltage (kV)	2.5-3	4.2

Table S2. HESI settings for HPLC-MS analyses

	HPLC
Syringe or mobile phase flow rate (µl/min)	170
Sheath gas flow (a.u)	50
Auxiliary gas flow (a.u)	3
Sweep gas flow (a.u)	0
Capillary temperature (°C)	300
Vaporizer temperature (°C)	150
Spray voltage (kV)	3.10